
Dating the Triassic continental rift in the southern Andes: the Potrerillos Formation, Cuyo Basin, Argentina

L.A. SPALLETTI^{|1|} C.M. FANNING^{|2|} and C.W. RAPELA^{|1|}

|1| **Centro de Investigaciones Geológicas, Facultad de Ciencias Naturales y Museo, Universidad Nacional de La Plata and CONICET**
Calle 1, nº 644, B1900 TAC, La Plata, República Argentina. Spalletti E-mail: spalle@cig.museo.unlp.edu.ar

|2| **Research School of Earth Sciences, The Australian National University**
Canberra, Australia

ABSTRACT

The Triassic successions of western Argentina commonly show thin pyroclastic levels intercalated within thick fluvial and lacustrine terrigenous deposits. The Potrerillos Formation is the thickest Triassic unit in the Cuyo Basin. It is composed of alternating cycles of gravelly- sandy- and muddy-dominated intervals, in which several laterally-continuous tuff horizons occur. U-Pb SHRIMP ages were determined on zircon grains from three tuff levels located between the lowermost and the middle sections of the Potrerillos Formation. The ages for the time of deposition of the tuffs are 239.2 ± 4.5 Ma, 239.7 ± 2.2 Ma and 230.3 ± 2.3 Ma (Middle Triassic). Chemical data indicate that these acid to intermediate volcaniclastic rocks are derived from coeval basic magmas displaying tholeiitic to slightly alkaline signatures. They are associated with the rift stage that followed the extensive post-orogenic volcanism of the Choiyoi Group, that in turn has been ascribed to slab break-off in neighbouring areas. Two of the studied samples also record a subpopulation of inherited zircon grains with crystallisation ages of 260-270 Ma. The latter are considered to be an indirect measurement for the age of the Choiyoi Group in the Cuyo basin. The rift-related Triassic event represents the culmination of the Gondwanian magmatic cycle, and is interpreted as the result of subduction cessation and anomalous heating of the upper mantle previous to the western Gondwana break-up.

KEYWORDS | Triassic. Cuyo Basin. Argentina. U-Pb zircon dating.

INTRODUCTION

The most important Triassic basins of southern South America are located near the Proto-Pacific margin of southwest Gondwana (Fig. 1). They are narrow and elongated depressions oriented NW-SE (Charrier, 1979), floored in most sectors by a widespread intraplate Upper Palaeozoic-Lowermost Triassic plutonic-volcanic com-

plex, the Choiyoi Group. The largest Triassic depocenter of western Argentina is the Cuyo Basin (Fig. 1). It covers an area of 40,000 km² and includes several fault-bounded subbasins filled with siliciclastic continental deposits. The Cuyo Basin may be characterised as a passive rift basin produced as a result of generalised extension induced by crustal thinning and collapse of the Upper Palaeozoic (Gondwana) orogen (Llambías and

Sato, 1990, 1995; Spalletti, 1999). It can be defined as a half graben that shows strong asymmetric structural and depositional features, as well as intrabasinal highs or transference zones that delimit different depocentres (Kokogian et al., 1988, 1993; Ramos and Kay, 1991; López Gamundí, 1994; Spalletti, 1999, 2001).

The volcaniclastic and sedimentary sequences of the Cuyo basin record complex interactions between alluvial, fluvial, deltaic and lacustrine depositional systems (Spalletti et al., 2005). These successions contain well-preserved fossil plants from numerous stratigraphic levels. This abundant and diverse floral record was essential in elucidating a comprehensive biostratigraphic chart for the Triassic continental successions (Spalletti et al., 1999; Morel et al., 2003; Artabe et al., 2007). However the absolute age of the Triassic record in the Cuyo Basin is a matter of debate. Stipanicic

(2001) and Stipanicic and Marsicano (2002) considered that most of the sediments were deposited during the Late Triassic. On the other hand, Spalletti et al. (1999), Spalletti (1999, 2001) and Morel et al. (2003) argued that the sedimentary infill of this basin embraced the whole Triassic. This fact emphasises the need of reliable chronostratigraphical markers. Fortunately, several ash fall tuff horizons occurred intercalated in the siliciclastic succession and provided the possibility of radiometric dating. The aim of this contribution is to document and describe three tuff horizons from the Triassic succession of the Cuyo Basin. We present new radiometric age data from SHRIMP U-Pb zircon dating together with new petrographic and whole-rock chemical information. This dataset is used to establish the composition of parental magmas, the tectonic signature of the pyroclastic materials, the age of primary and secondary zircon grains, and the precise chronostratigraphic location of palaeofloral levels.

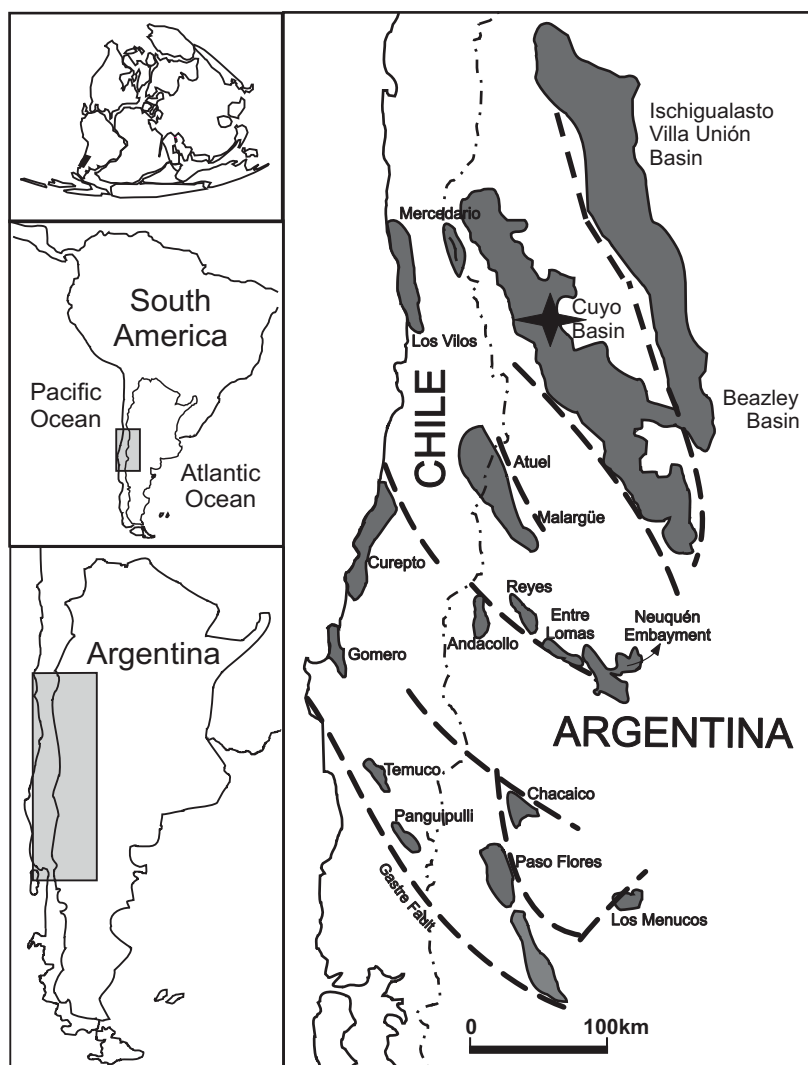


FIGURE 1 | Map of central Argentina and Chile showing the main Triassic basins and depocentres (after Morel et al., 2003).

GEOLOGICAL BACKGROUND

The Triassic sediments of the Cuyo Basin only crop out along the northwestern sector of the basin in the Precordillera geological province. Potrerillos (Fig. 2) is a classic locality for the study of the Triassic deposits of the Cuyo Basin because the whole Triassic Uspallata Group (Stipanicic, 1979) is exposed. From base to top it is made up of the Río

Mendoza, Cerro de Las Cabras, Potrerillos, Cacheuta and Río Blanco Formations (Fms) (Fig. 2). Although these deposits have been extensively studied from the stratigraphic point of view, only recently Spalletti et al. (2005) and Artabe et al. (2007) have provided detailed information on sedimentary facies, depositional systems and their rich palaeobotanical record.

The lowermost Río Mendoza Fm (314 m thick) unconformably overlies volcanic and volcaniclastic deposits of the Choiyoi Group. It is composed of thick tabular and lenticular bodies of volcaniclastic, poorly mature conglomerates and agglomerates with a generalised fining upward stacking pattern. The overlying Cerro de Las Cabras Fm is a 190 m thick unit. Its lower part is a mud-rich succession with intercalated lenticular bodies of conglomerates and pebbly sandstones. The upper section is a fine-grained succession composed of multicoloured mudstones, tuffs and pyroclastic siltstones. The Potrerillos Fm is the thickest Triassic unit (735 m) and is characterised by cyclic alternations of gravel-, sand- and mud-rich intervals. These deposits are followed by a 44 m thick succession of black shales of the Cacheuta Fm. The Triassic succession ends with the 231 m thick red beds of the Río Blanco Fm.

One of the most important palaeofloral Triassic records of Argentina (13 fossil horizons with 23 taxa) is recognised in the Potrerillos Fm (Spalletti et al., 2005; Artabe et al., 2007). According to the biostratigraphic chart based on plant megafossils proposed by Spalletti et al. (1999), two assemblage biozones (MBC and BNP) are identified in the type locality of the Potrerillos Fm (Fig. 3). This biostratigraphic information allowed Spalletti et al. (1999) and Morel et al. (2003) suggest that the Potrerillos Fm was deposited during the late Middle Triassic - early Late Triassic (Fig. 3).

In the studied section of the Potrerillos Fm, airfall tuffs and re-sedimented pyroclastic deposits are intercalated within the conglomerates, sandstones and shales. Tuffs and tuffaceous sedimentary rocks usually make up a subordinate proportion of the sedimentary record. These deposits are typically thin (< 1.5 m), fine-grained, vitric, unwelded and weakly consolidated. One of the three ash fall tuff beds sampled for petrographic, chemical and geochronological analysis (sample PTR 0) is located near the base of the Potrerillos Fm (Fig. 4). The other two samples (PTR 1 and PTR 2) have been taken from the middle part of this stratigraphic unit, below and above the main (1 to 10) palaeofloral horizons (Fig. 4).

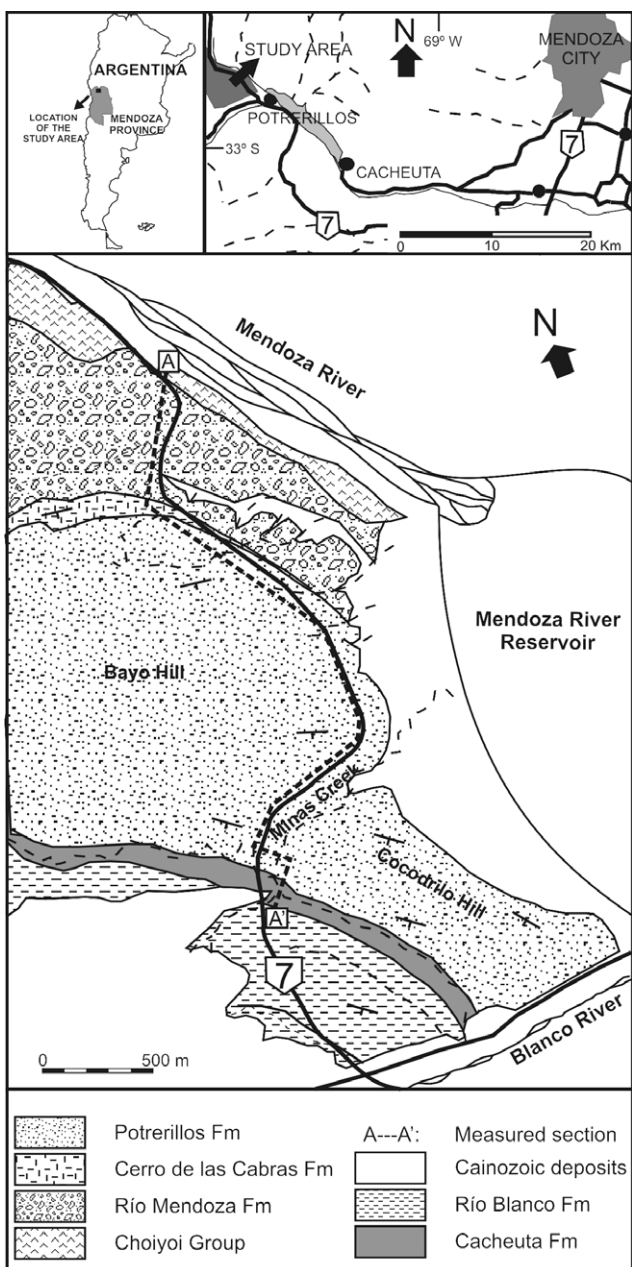


FIGURE 2 | Location map and geological map of the Potrerillos area. Modified after Días and Massabie (1974).

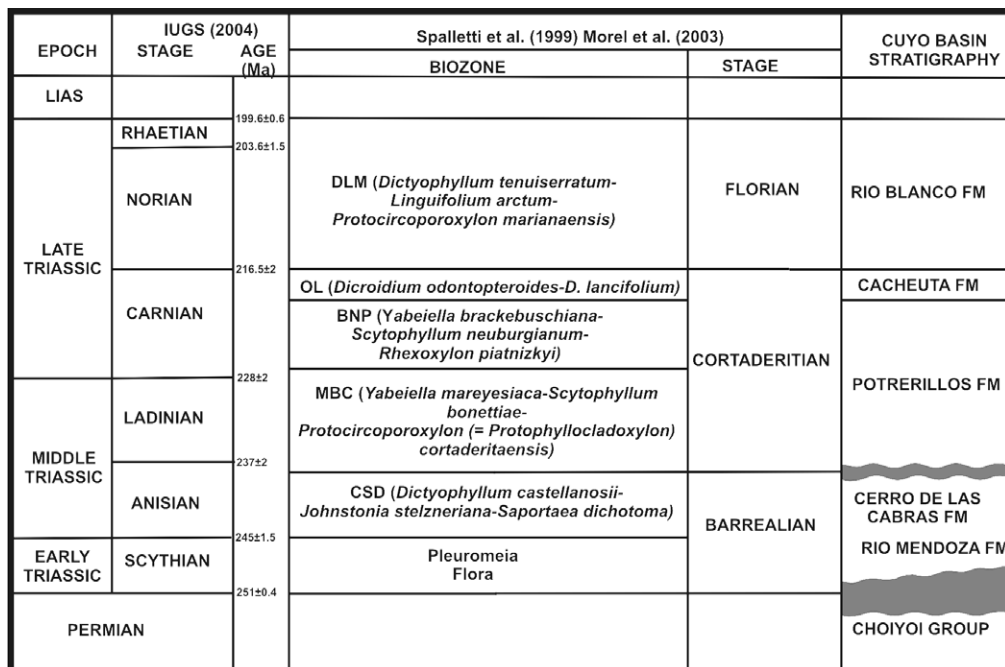


FIGURE 3 | Biostratigraphic and chronostratigraphic chart of the Triassic deposits of the Cuyo Basin, modified from Spalletti et al. (1999) and Morel et al. (2003).

SAMPLE PREPARATION, ANALYTICAL METHODS

Only fresh material was collected where possible and any remaining weathered material was removed before crushing. Chemical analyses for major and minor elements were obtained for all the samples from ACTLABS, Canada. Samples were pulverized in mild steel and processed by ICP and ICP/MS. Full chemical data are given in Table 1 (see p. 280).

For geochronological analysis, crushed samples were lightly milled in a tungsten-carbide ring mill such that all material passed through a 60 BSS mesh nylon sieve, and heavy minerals were concentrated by standard heavy liquid and magnetic separation techniques. Zircon grains were hand-picked and mounted in epoxy resin with chips of the FC1 and SL13 reference zircons, and then polished down to expose the grain mid-sections. Reflected and transmitted light photomicrographs, and cathodoluminescence (CL) SEM images were prepared for all zircons. The CL images were used to decipher the internal structures of the sectioned grains and to target specific areas within the zircons.

The U-Th-Pb analyses were made using SHRIMP II at the Australian National University, each analysis consisting of 6 scans through the mass range. The data have been reduced in a manner similar to that described by Williams (1998, and references therein), using the

SQUID Excel Macro of Ludwig (2001). The Pb/U ratios were normalised relative to a value of 0.1859 for the $^{206}\text{Pb}/^{238}\text{U}$ ratio of the FC1 reference zircons, equivalent to an age of 1099 Ma (see Paces and Miller, 1993). Uncertainties given for individual analyses (ratios and ages) are at the one sigma level; however the uncertainties in calculated weighted mean ages are reported as 95% confidence limits. Tera and Wasserburg (1972) concordia plots, relative probability plots with stacked histogram and weighted mean $^{206}\text{Pb}/^{238}\text{U}$ age calculations were carried out using ISOPLOT/EX (Ludwig, 2003).

SAMPLE DESCRIPTION

Sample PTR 0

The lower section of the Potrerillos Fm is almost entirely dominated by thick conglomerates deposited by sheet floods, stream floods and debris flows in an alluvial depositional system. The sample PTR 0 was taken from a tuff bed located 4 m above the base of the Potrerillos Fm (Fig. 4). It is a 0.5 m thick felsic fine-grained tuff horizon that is interbedded with terrigenous mudstones and fine-grained sandstones that intercalate within the conglomeratic succession. Single crystals and crystal fragments of angular volcanic quartz (8%) and unaltered Na-plagioclase (5%) constitute only a small proportion of the rock. The tuff contains a significant amount (12%) of accessory

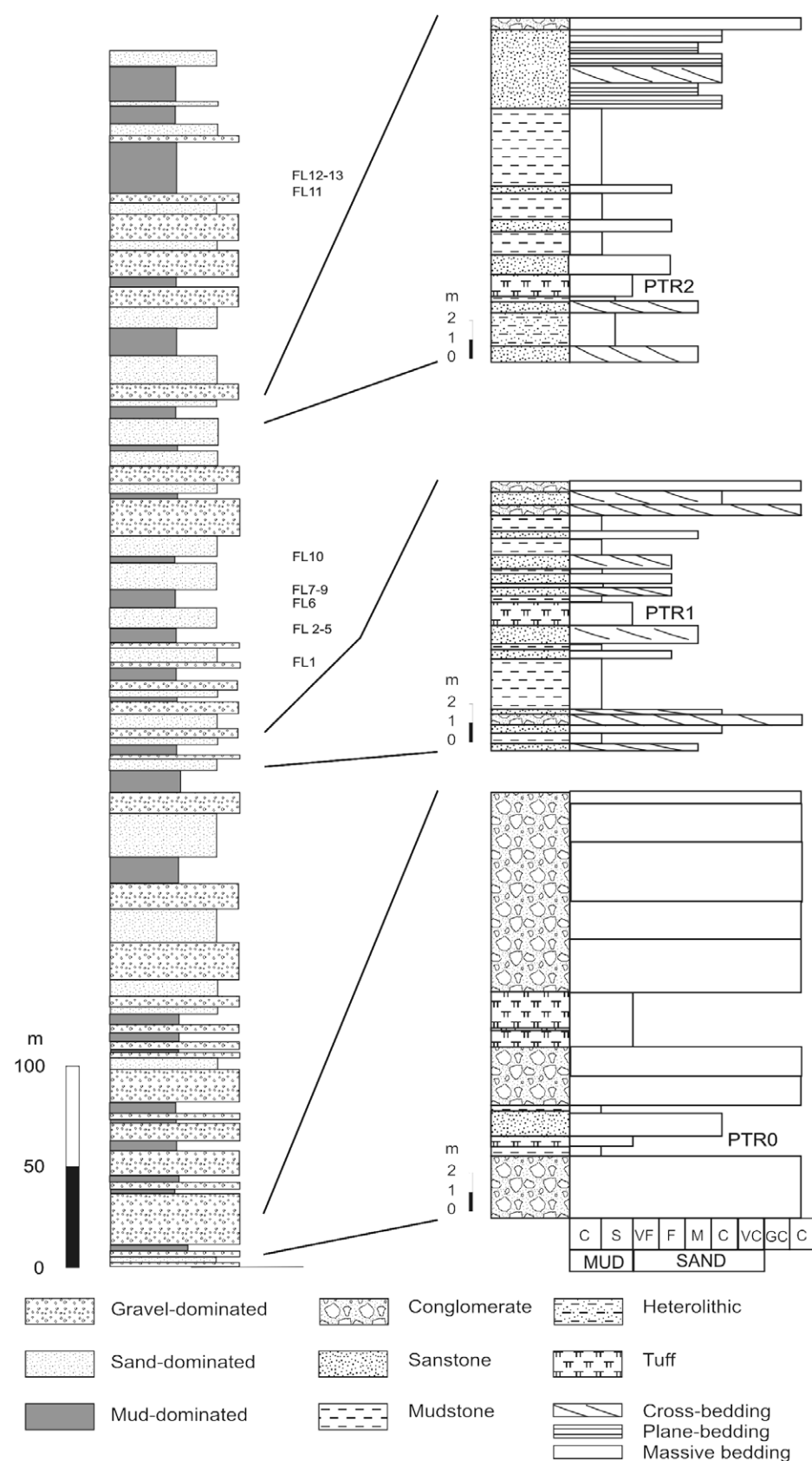


FIGURE 4 | Simplified log of the Potrerillos Formation showing the location of the studied tuffs and floristic levels.

grains (including sub-rounded clasts of K-feldspar altered to clay-minerals, and coarse-grained volcanic and pyroclastic rock fragments) that were probably entrained during explosive volcanism. Some of the zircons recovered from this sample are accessory components. The tuff sample also contains a few non-volcanic quartz and K-feldspar grains. The abundant matrix (80%) consists of microcrystalline quartz, feldspar and glass shards which are mostly altered to smectite and kaolinite.

Sample PTR 1

PTR 1 is a sample of a 1.2 m thick pyroclastic deposit located 267 m above the base of the Potrerillos Fm (Fig. 4). This level is associated with cross-stratified and horizontal-laminated volcaniclastic sandstones and massive mudstones interpreted as the deposits of a mixed-load fluvial system. This tuff was originally an airfall deposited in a flood plain setting with minimal re-sedimentation (in the sense of Blake et al., 2004). A very fine-grained vitric matrix comprises 95 vol.% of the total sediment, and is composed of almost unaltered platy and parallel-oriented glass shards. Quartz splinters (up to 200 μm) and tabular Na-plagioclase crystals (250–300 μm) are scarce (<4%). This tuff contains a small component of accidental rounded and sub-rounded rhyolitic volcanic rock fragments. As in the case of sample PTR 0, the zircon grains recovered from this specimen are interpreted to be part of the accessory component.

Sample PTR 2

PTR 2 was sampled from a 1.2 m thick massive vitric-crystalline tuff located 436 m above the base of the Potrerillos Fm (Fig. 4). This primary pyroclastic deposit is interbedded with terrigenous cross-stratified sandstones, massive sandstones and mudstones formed in a mixed-load fluvial system. Juvenile pyroclasts of subhedral volcanic quartz and Na-plagioclase (300–900 μm) constitute about 65% of the total rock. Elongated biotite crystals, regarded as juvenile detrital components, are less common. A small proportion (< 6%) of accidental volcanic and pyroclastic rock fragments was identified. The matrix of this tuff is composed of almost unaltered very fine-grained glass shards. Mesogenetic calcite spar appears as patches, partially replacing the original vitric matrix.

CHEMICAL COMPOSITION

The tuffs have an overall subalkaline chemical composition with SiO_2 between 62 and 74%, $(\text{Na}_2\text{O} + \text{K}_2\text{O})$ at 4.7–6.4 % and $(\text{FeO} + \text{MgO})$ contents of 1.0–3.2% (Table 1). REE patterns have $[\text{La}/\text{Yb}]_N$ of 6–9, but while

PTR0 and PTR1 have a negative Eu anomaly ($\text{Eu}/\text{Eu}^* = 0.6$ –0.7), PTR2 displays a MREE depletion without a Eu anomaly (Fig. 5). This is usually related to amphibole fractionation in intermediate and silicic compositions, because of the high MREE mineral/melt partition coefficients in these magmas (e.g. Henderson, 1982).

The Chemical Index of Alteration (CIA, Nesbitt and Young, 1982) ranges from 64.4 to 72.9 (Table 1), suggesting that the tuffs were affected by chemical alteration to a moderate degree. PTR 0 exhibits the highest values of Al_2O_3 and CIA as a result of alteration of volcanic glass to clay minerals. In the case of sample PTR 2 the presence of calcite as a secondary phase contributed to the reduction of the CIA value.

The total alkali content and the silica content of samples PTR 0, PTR 1 and PTR 2 have values that are typical

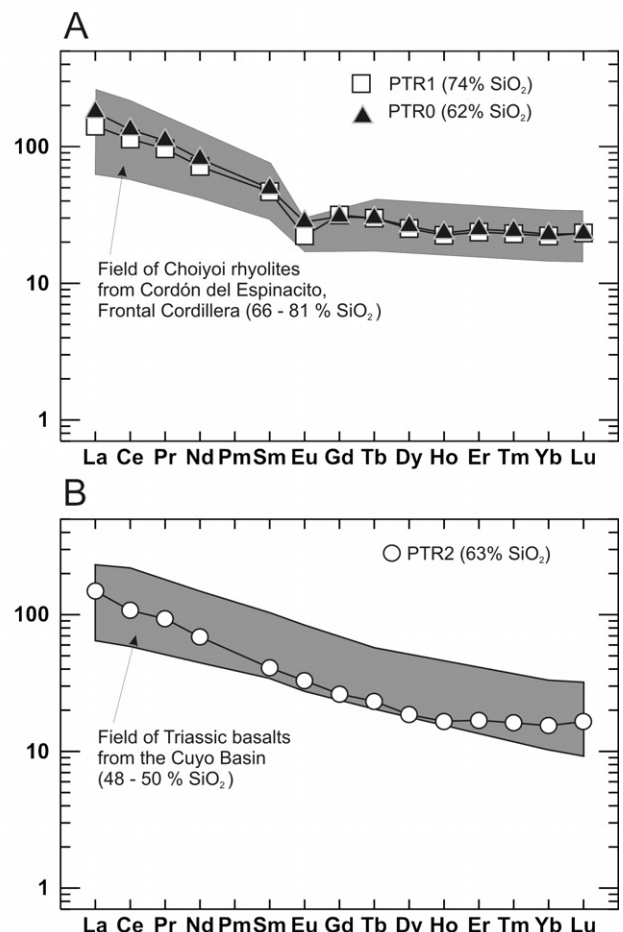


FIGURE 5 | Chondrite-normalized REE elements patterns (Taylor and McLennan, 1985) for the pyroclastic samples of the Potrerillos Formation. A) Relationship between the REE patterns of samples PTR 0 and PTR 1 and the Choioyi rhyolites of Cordón del Espinacito (data from Pérez and Ramos, 1996). B) Relationship between the REE pattern of sample PTR 2 and the Triassic basalts of the Cuyo Basin (data from Ramos and Kay, 1991).

for andesite, rhyolite and low-silica dacite, respectively (Fig. 6A), although the original alkali content might have been modified to some degree by secondary alteration. A classification based on ratios of the relative immobile elements such as Zr, TiO₂, Nb and Y point to a rhyodacitic – dacitic composition for these pyroclastic rocks (Fig. 6B). Tectonic discrimination diagrams show that the Potrerillos tuffs plot in the magmatic arc field, close to the boundary with intraplate granites (Fig. 7). Further, on a La/Ta vs. Ba/Ta diagram (Kay and Mpodozis, 2002) the studied samples fall in an intermediate position between backarc and arc signatures (Fig. 8).

GEOCHRONOLOGICAL RESULTS

Geochronological results are summarised in Tables 2, 3 and 4 (see p. 281-283), and Fig. 9.

Sample PTR 0

The zircon grains are mostly euhedral elongate to equant in shape, with some slender elongate grains (Fig. 10). The majority of the grains are around 100 µm in length, though range from about 50 µm to greater than 200 µm. Many have bipyramidal terminations, though some have round terminations interpreted to result from surface transport. A few of the more elongate grains have central cavities that are interpreted to be trapped gas vapour trails, resulting from rapid crystallisation. The CL images show a dominantly simple, oscillatory zoned, igneous internal structure (Fig. 10). A number of grains have large, broad zones, perhaps reflecting zircon that has crystallised from a more mafic magmatic source. Inherited zoned magmatic components are present in the central areas of some grains.

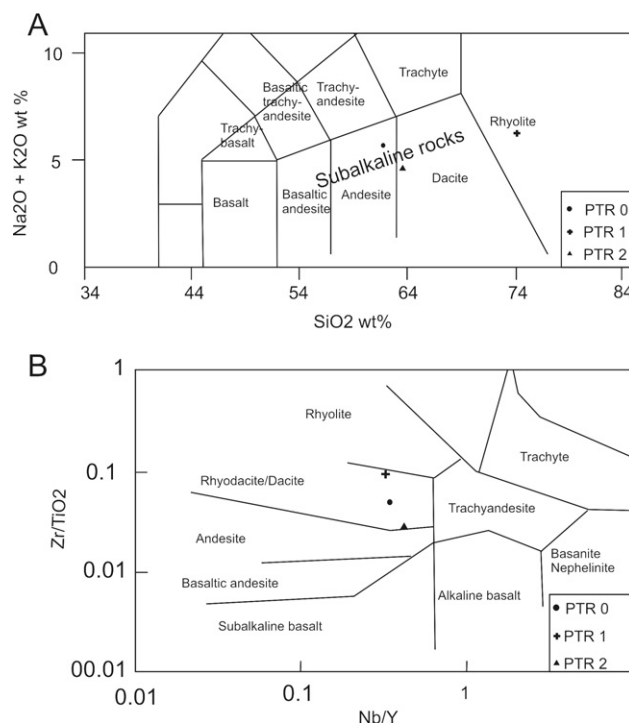


FIGURE 6 | A) Silica versus total alkali diagram and chemical classification of volcanic rocks (after Le Maitre et al., 1989). The Potrerillos Formation tuffs vary in composition from andesite (PTR 0) to rhyolite (PTR 1). B) Nb/Y versus Zr/TiO₂ diagram and chemical classification of the volcanic rocks (after Winchester and Floyd, 1977). The three pyroclastic samples of the Potrerillos Formation plot in the rhyodacite/dacite field.

Twenty eight grains have been analysed (Table 2, Fig. 9A). The U concentrations are variable, from 13 to 310 ppm. Th varies sympathetically with U and the Th/U ratios are relatively constant at about 0.4 to 0.8. The Pb

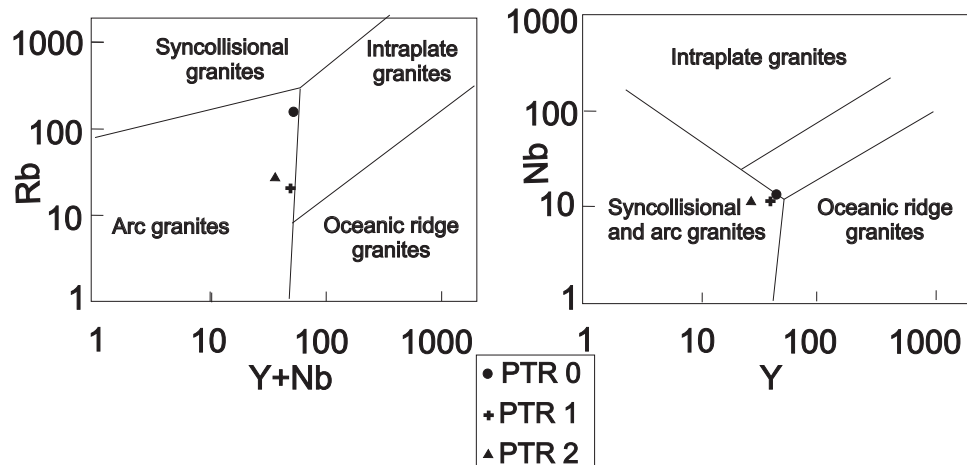


FIGURE 7 | Y+Nb versus Rb and Y versus Nb plots (Pearce et al., 1984) for the tuffs of the Potrerillos Formation. The three samples fall in the volcanic arc granite field close to the boundary with the intraplate granite field.

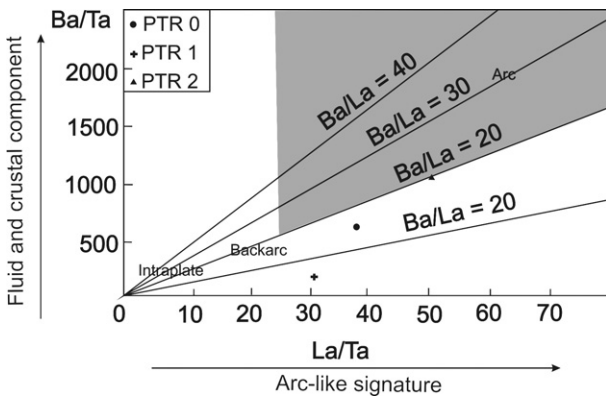


FIGURE 8 | Plot of La/Ta versus Ba/Ta (Kay and Mpodozis, 2002). The Potrerillos tuffs plot in an intermediate position between backarc and arc signatures.

data form a dispersed pattern on the Tera-Wasserburg plot, and whilst most are low in common Pb, 5 of the areas analysed are more enriched (Table 2). On a probability density plot the data form a series of age peaks or groupings. The dominant group has a bimodal age distribution in the range ~250 Ma to ~270 Ma, with minor grains ranging to ~280 Ma. There is a solitary analysis at about 320 Ma and 4 grains with $^{206}\text{Pb}/^{238}\text{U}$ of about 240 Ma. The major group of analyses can be deconvolved into two distinct age peaks at 258 ± 4 Ma and 267 ± 4 Ma. For the youngest 4 analyses, a weighted mean of the $^{206}\text{Pb}/^{238}\text{U}$ ages gives 239.2 ± 4.5 Ma (MSWD = 0.15). Given that all grains analysed are zoned igneous zircons, and that the rock is a volcaniclastic, it is interpreted that this youngest coherent age grouping, albeit of 4 grains, places a maximum age constraint on the time of deposition of this tuffaceous rock.

Sample PTR 1

The zircon grains from this sample are variable in size, ranging from equant types about $50\mu\text{m}$ in diameter to elongate grains around $200\mu\text{m}$ in length (Fig. 11). Many have bipyramidal terminations, others are broken fragments of such grains. The CL images reveal a dominantly simple oscillatory zoned internal structure, though some grains are sector zoned, whilst others have inherited centres (Fig. 9).

Twenty grains have been analysed (Table 3, Fig 9B). As noted above for sample PTR0, there is a marked range in U concentrations, from 14 to 363 ppm, with one area having about 700 ppm U. The Th/U ratios are similarly variable but generally greater than 0.6, ranging to 1.8. On the Tera-Wasserburg plot, the analysis of grain 1 (with ~14 ppm U) is notably enriched in common Pb; the others from a dispersed pattern close to or within uncertainty of the Concordia curve. The relative probability plots show

two distinct age groupings; a dominant peak at about 240 Ma with a shoulder on the older age side, and a lesser peak at about 270 Ma. A weighted mean for the 11 analyses comprising the dominant age group gives a $^{206}\text{Pb}/^{238}\text{U}$ age of 239.7 ± 2.2 Ma (MSWD = 0.68). This is interpreted as the crystallisation age of this zoned igneous zircon group, and constrains the maximum age of deposition for this pyroclastic rock. Using the mixture modelling algorithm it is possible to deconvolute the age populations into a possible group at about 250 Ma (i.e. the “shoulder”) and a significant older group at 268 ± 4 Ma, and (Table 3, Fig. 9B).

Sample PTR 2

The zircons are dominantly euhedral elongate grains with pyramidal terminations, or fragments of such grains. There are a few more equant grains, but most are elongate (in the order of $200\mu\text{m}$ in length) and many have central cavities consistent with rapid cooling in a volcanic to sub-volcanic setting (Fig 12). The CL images show oscillatory zoning from centre to rim, consistent with crystallisation during a single igneous event (Fig 12).

Twenty areas have been analysed (Table 4, Fig 9C). The areas analysed have notable uniform U concentrations, most between 55 and 90 ppm, and the Th is similar with relatively high Th/U ratios predominantly between 0.8 and 1.2. All 20 analyses form a single coherent cluster on the Tera-Wasserburg plot and a simple bell-shaped curve on the probability density plot. A weighted mean of the $^{206}\text{Pb}/^{238}\text{U}$ ages for all 20 lacks excess scatter giving 230.3 ± 2.3 Ma (MSWD = 1.07). This weighted mean age is interpreted to constrain the time of eruption and so the effective age of deposition for the tuff.

DISCUSSION AND CONCLUSIONS

Thin tuff bands (samples PTR 0, PTR 1 and PTR 2) interbedded in the siliciclastic deposits of the Potrerillos Fm and located between the base and the middle part of this stratigraphic unit have absolute ages for the time of eruption and deposition of 239.2 ± 4.5 Ma, 239.7 ± 2.2 Ma and 230.3 ± 2.3 Ma (Middle Triassic). The interpreted age for sample PTR 0 (239.2 ± 4.5 Ma) constrains the onset of sedimentation of the Potrerillos Fm, and according to the International Stratigraphic Chart (2004) the lower part of the Potrerillos Fm must be dated in the earliest Middle Triassic. This is consistent with the Early Triassic U-Pb SHRIMP dating of the underlying Río Mendoza Fm at the base of the Uspallata Group (243 ± 4.7 Ma, Ávila, 2003; Ávila et al., 2003, 2006). The 235 ± 5 Ma, K-Ar whole rock age obtained in a basaltic sill intruded in the Cerro de las Cabras Fm (Ramos and Kay, 1991),

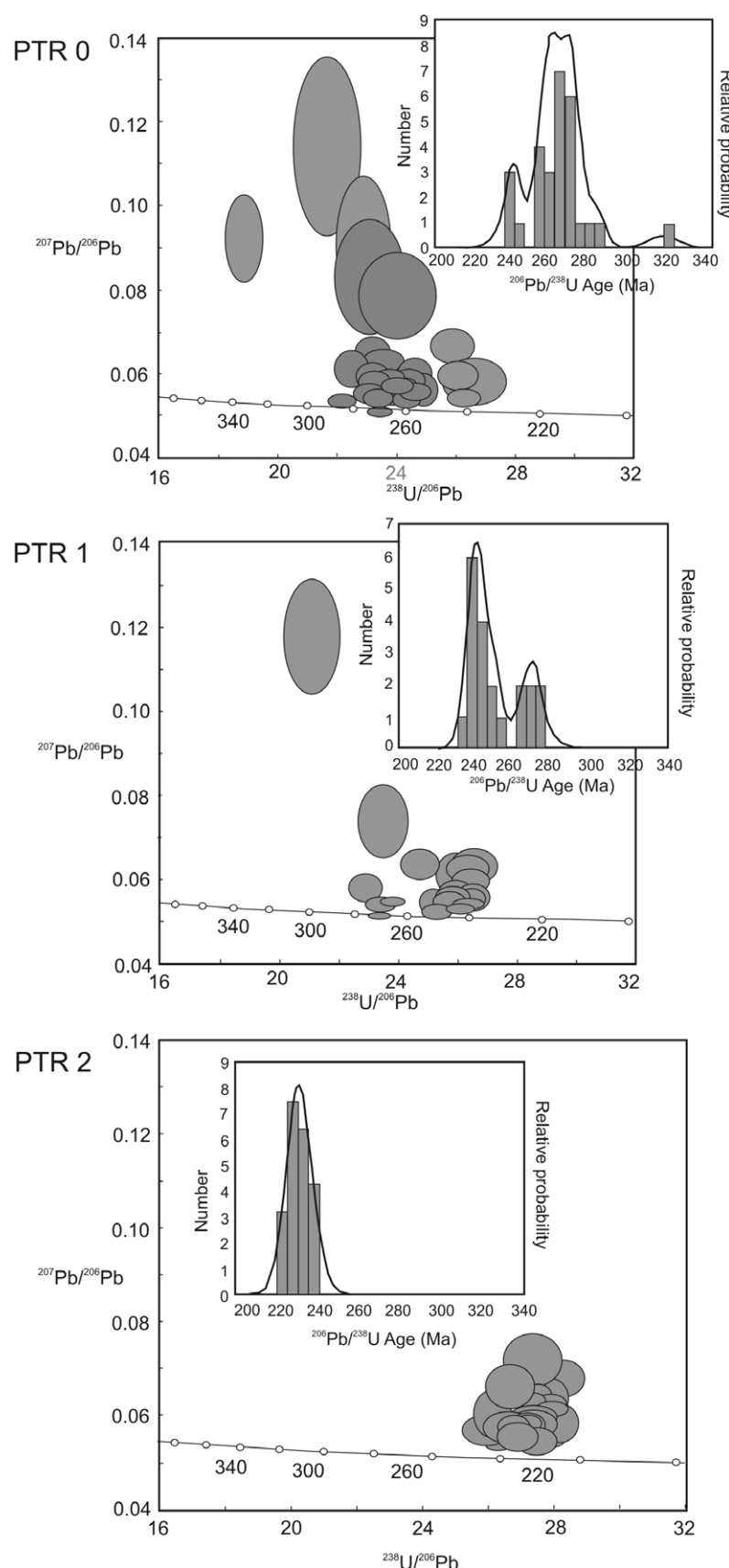


FIGURE 9 | Tera-Wasserburg and probability plots of U-Pb SHRIMP zircon-dating results for tuffs of the Potrerillos Formation.

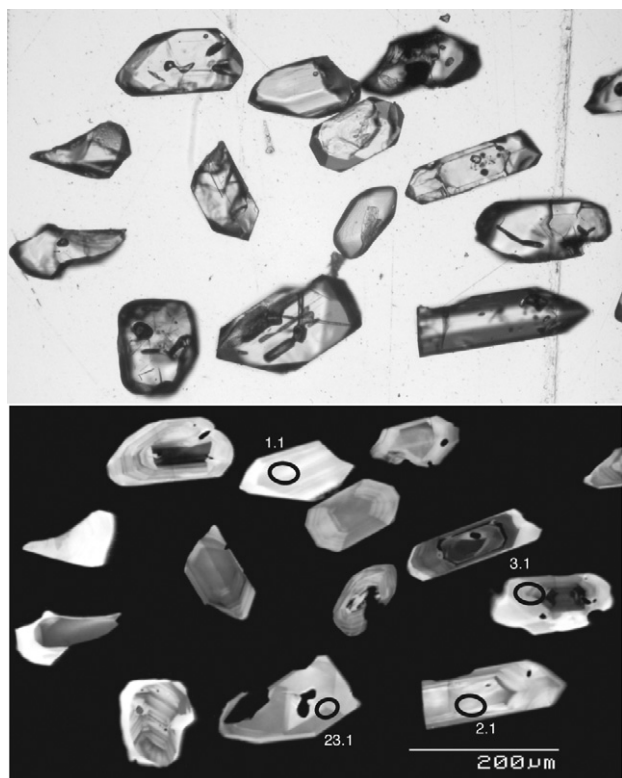


FIGURE 10 | Photomicrographs of mounted zircon grains from sample PTR 0, lowermost levels of the Potrerillos Formation. Above transmitted light photomicrographs, below cathodoluminescence (CL) SEM image. Note the co-existence of euhedral, fractured and rounded zircon grains.

that underlay the Potrerilllos and overlay the Río Mendoza formations, is in turn younger and not consistent with the stratigraphic position of this unit.

In PTR 0 and PTR 1 the zoned igneous zircons that record Permian crystallisation ages of about 260 to 270 Ma are consistent with derivation from equivalent aged volcanic rocks (the Permian Choiyoi Group). Whilst no clear core-rim structures are present, nor have been analysed, it is probable that these discrete and coherent older zircon grains were incorporated into the volcanioclastic rocks during eruption and deposition, rather than having been derived from the source of the magma. The whole-rock REE patterns for these samples are consistent with this interpretation, as they resemble those of the underlying Choiyoi volcanic rocks (Fig. 5A). Therefore the ages of about 260 – 270 Ma may represent an indirect measurement for the Choiyoi crystallisation age in this area. Precise ages of the Choiyoi group in this sector are unknown. However, the age is in agreement with the K/Ar age of 275 ± 10 Ma obtained by Vilas and Valencio (1982) for volcanioclastic rocks of the Choiyoi Group in the Frontal Cordillera (to the west of the studied area). Furthermore, equivalent acid plutonic-volcanic complexes

in northern Patagonia have U-Pb SHRIMP ages between 246 and 273 Ma (La Esperanza area, Pankhurst et al., 2006).

The tuff sample PTR 2, located in the upper middle third of the Potrerillos Fm, was deposited during the uppermost Middle Triassic (230.3 ± 2.3 Ma). The REE pattern is similar to the patterns of basic volcanic rocks of Triassic age in the Cuyo Basin (Fig. 5B). The depletion of MREE in PTR2 ($\text{SiO}_2 = 63.7\%$) suggests that these intermediate pyroclastic rocks are the result of fractionation of parental magmas with 48-50 % SiO_2 (Fig. 5B) with tholeiitic to slightly alkaline signatures (Ramos and Kay, 1991).

This restricted magmatism associated with the Triassic rift basins represents the last stage of the “Gondwanian” orogenic cycle of the Southern Andes and Patagonia (Pankhurst and Rapela, 1998). This cycle started with subduction-related magmatism in the Lower Carboniferous. It was followed by Late Carboniferous compressive deformation and associated peraluminous magmatism, and Early Permian extensive post-orogenic plutonic-

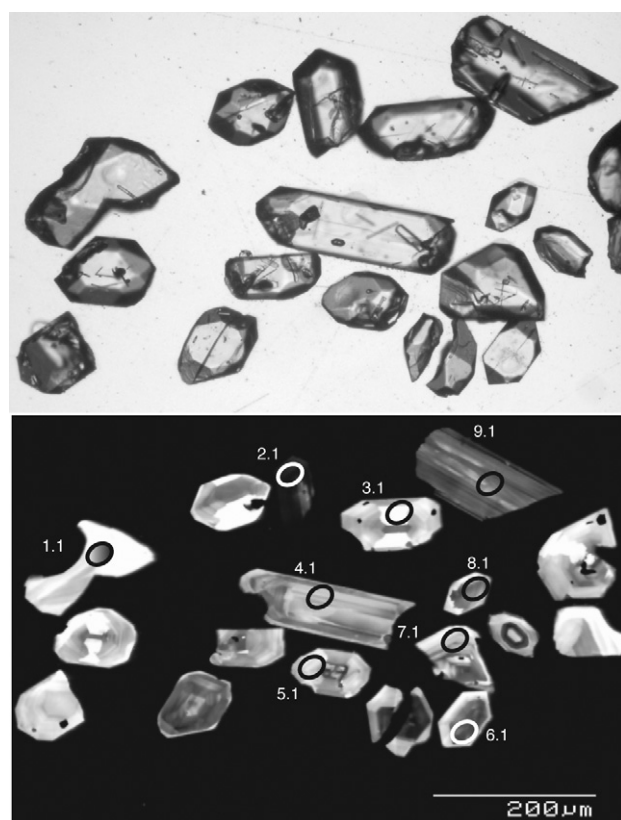


FIGURE 11 | Photomicrographs of mounted zircon grains from sample PTR 1. Above transmitted light photomicrographs, below CL image. Most of the zircon grains are euhedral and show well developed magmatic zoning.

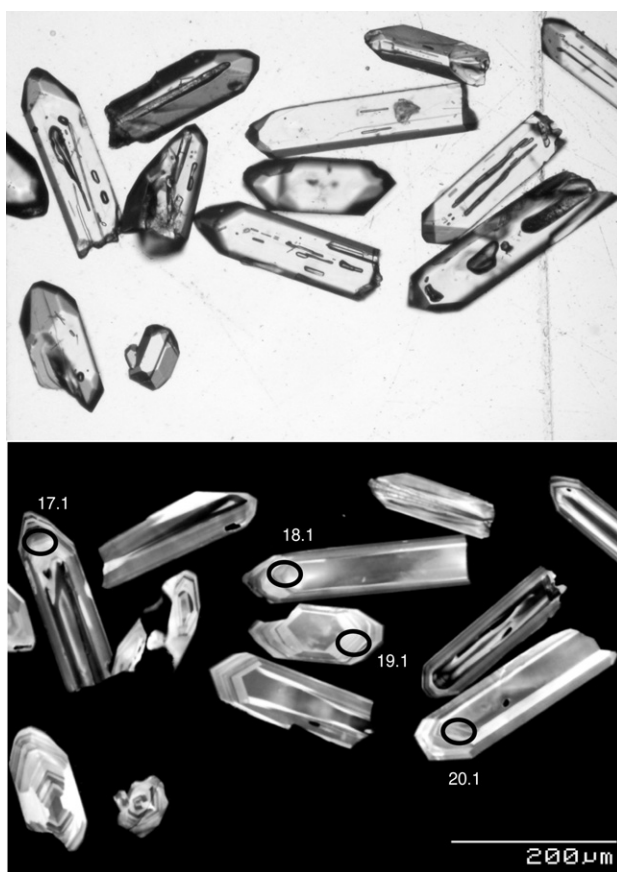


FIGURE 12 | Photomicrographs of mounted zircon grains from sample PTR 2. Above transmitted light photomicrographs, below CL image. Zircon faces are well developed and not abraded.

volcanic complexes (Choiyoi group) interpreted as slab break-off magmatism (Pankhurst et al. 2006, and references therein). However, a geochemical study of the Choiyoi volcanics in the Mendoza Province Precordillera (Strazzere et al., 2006) suggests that subduction-related arc magmatism with minor within-plate component extended from Early to Late Permian times.

The Triassic rifting is closely linked to structures created by previous tectonothermal episodes such as the development of a Carboniferous-Permian orogenic belt and to events along the proto-Pacific margin of Gondwana (Fig. 13; Franzese and Spaletti, 2001). The cessation of Upper Palaeozoic subduction, coeval with establishment of dextral strike slip tectonics parallel to the continental margin, caused detachment of the subducting slab and generation of an asthenospheric window (Fig. 13). Thus, anomalous heating of the upper mantle resulted in bimodal magmatism, uplift, thermal weakening and gravitational collapse of the upper crust. As shown by Franzese and Spaletti (2001) this extension is not related to the tectonics that caused the later break-up of Gondwana.

The SHRIMP ages presented in this paper clearly confirm that the correct stratigraphic location of the Potrerillos Fm is within the time frame of Middle Triassic - earliest Late Triassic. The ten fossiliferous levels between the stratigraphic positions of samples PTR 1 and PTR 2

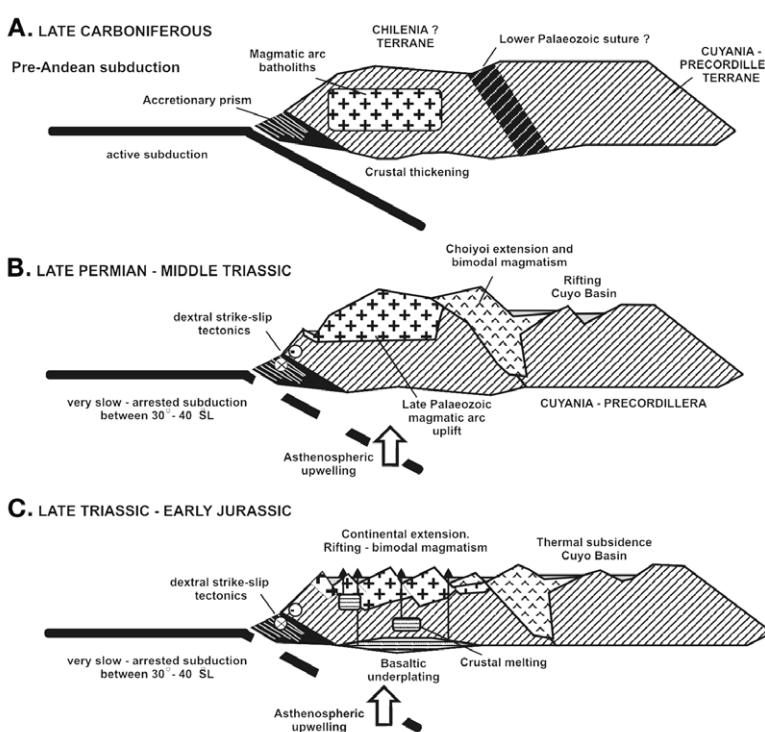


FIGURE 13 | Sketch cross section of the western Gondwana margin around 37° S showing the Upper Paleozoic to Lower Jurassic tectonic evolution of the Andean region (modified from Franzese and Spaletti, 2001).

belong to the assemblage biozone MBC (*YabeIELLA mereyesiaca* - *Scytophyllum bonettiae* - *Protophyllocladoxylon cortaderitaensis*, Spalletti et al. 2005). According to the U-Pb zircon ages of samples PTR 1 and PTR 2, this paleobotanical record must be dated as Middle Triassic. Further, the three fossiliferous levels located at the uppermost Potrerillos Formation above PTR 2 belong to the BNP biozone (*YabeIELLA brackebuschiana* - *Scytophyllum neuburgianum* - *Rhexoxylon piatnitzkyi*, Spalletti et al., 2005) which is clearly of a Late Triassic age.

These Triassic fossil floras have a remarkable continuity in different continental depocentres of western Gondwana (Morel et al., 2003). Therefore the more accurate dating of the main Assemblage Biozones of the Triassic of west-central Argentina and the adjusted chronostratigraphic chart proposed in this paper may be used as a reference for long-distance correlations.

ACKNOWLEDGEMENTS

The authors would like to thank Robert J. Pankhurst, Carita Augutsson and Lluís Cabrera for many constructive comments that improved an earlier version of this article.

REFERENCES

- Artabe, A., Morel, E., Ganuza, D., Zavattieri, A., Spalletti, L., 2007. La paleoflora triásica de Potrerillos, provincia de Mendoza, Argentina. *Ameghiniana*, 279-301.
- Ávila, J.N., 2003. Evolução tectono-termal-deposicional da sub-bacia de Cacheuta, bacia de Cuyo, NW-Argentina. Instituto de Geociências, Universidade Federal do Rio Grande do Sul. Trabalho Conclusão Curso Geologia, Porto Alegre, 132 pp.
- Ávila, J.N., Chemale Jr. F., Cingolani, C.A., Armstrong, R., Kawashita, K., 2003. Sm-Nd isotopic signature and U-Pb Shrimp zircon dating of the Cacheuta Sub-Basin, Cuyo Basin, NW-Argentina. IV American Symposium on Isotope Geology, Salvador, Abstracts, 35-37.
- Ávila, J.N., Chemale Jr. F., Mallmann, G., Kawashita, K., Armstrong, R., 2006. Combined stratigraphic and isotopic studies of Triassic strata, Cuyo Basin, Argentine Pre-cordillera. *Geological Society of America Bulletin*, 118, 1088-1098.
- Blake, T.S., Buick, R., Brown, S.J.A., Barley, M.E., 2004. Geochronology of a Late Archean flood basalt province in the Pilbara Craton, Australia: constraints on basin evolution, volcanic and sedimentary accumulation, and continental drift rates. *Precambrian Research*, 133, 143-173.
- Charrier, R., 1979. El Triásico en Chile y regiones adyacentes de Argentina: una reconstrucción paleogeográfica y paleoclimática. *Comunicaciones*, 26, 1-37.
- Días, H.D., Massabie, A., 1974. Estratigrafía y tectónica de las sedimentitas triásicas, Potrerillos, provincia de Mendoza. *Revista de la Asociación Geológica Argentina*, 29, 185-204.
- Franzese, J., Spalletti, L., 2001. Late Triassic – Early Jurassic continental extension in southwestern Gondwana: tectonic segmentation and pre break-up rifting. *Journal of South American Earth Sciences*, 14, 257-270.
- Henderson, P., 1984. General geochemical properties and abundances of the Rare Earth Elements. In: Henderson, P. (ed.). *Rare Earth Element Geochemistry*. Elsevier, Amsterdam, 510 pp.
- Kay, S.M., Mpodozis, C., 2002. Magmatism as a probe to the Neogene shallowing of the Nazca plate beneath the modern Chilean flat-slab. *Journal of South American Earth Sciences*, 15, 39-57.
- Kokogán, D.A., Boggetti, D.A., Rebay, G., 1988. Cuenca Cuyana. El análisis estratigráfico secuencial en la identificación de entrampamientos sutiles. Congreso Nacional Exploración de Hidrocarburos, Buenos Aires, Actas, 1, 649-674.
- Kokogán, D.A., Fernández Seveso, F., Mosquera, A., 1993. Las secuencias sedimentarias triásicas. In: Ramos, V.A. (ed.). *Relatorio Geología y Recursos Naturales de Mendoza. 12º Congreso Geológico Argentino, 2º Congreso de Exploración de Hidrocarburos*, Buenos Aires, 65-78.
- Llambías, E., Sato, A., 1990. El Batolito de Colanguil (29-31°S) Cordillera Frontal de Argentina: estructura y marco tectónico. *Revista Geológica de Chile*, 17, 89-108.
- Llambías, E., Sato, A., 1995. Tectónica y magmatismo en el límite Pérmico - Triásico de la Cordillera Frontal. Reunión Triásico del Cono Sur, Bahía Blanca, Actas, 2, 22-26.
- Le Maître, R.W., Bateman, P., Dubek, A., Keller, J., Lameyre, J., Le Bas, M.J., Sabine, M.A., Schmid, D., Sorensen, H., Streckeisen, A., Woolley, A.R., Zanettin, B. (Eds.), 1989. *A Classification of Igneous Rocks and Glossary of Terms: Recommendations of the International Union of Geological Sciences Subcommission on the Systematics of Igneous Rocks*. Blackwell Science, Oxford, 193 p.
- López Gamundi, O., 1994. Facies distribution in an asymmetric half graben: the northern Cuyo Basin (Triassic), western Argentina. 14th International Sedimentological Congress Recife S1, Abstracts, 6-7.
- Ludwig K.R., 2001. SQUID 1.02, A User's Manual. Berkeley Geochronology Center Special Publication, No. 2, 17 pp.
- Ludwig, K.R., 2003. User's manual for Isoplot/Ex, Version 3.0. A geochronological toolkit for Microsoft Excel. Berkeley Geochronology Center Special Publication, No. 4, 70 pp.
- Morel, E., Artabe, A., Spalletti, L., 2003. The Triassic floras of Argentina: biostratigraphy, floristic events and comparison with other areas of Gondwana and Laurasia. *Alcheringa* 27, 231-243.
- Nesbitt, H.W., Young, G.M., 1982. Early Proterozoic climates and plate motions inferred from major element chemistry of lutites. *Nature*, 299, 715-717.
- Paces, J.B., Miller, J.D., 1993. Precise U-Pb ages of Duluth Complex and related mafic intrusions, northeastern Min-

- nesota: geochronological insights to physical, petrogenetic, paleomagnetic, and tectonomagmatic process associated with the 1.1 Ga Midcontinent Rift System. *Journal of Geophysical Research*, 98B, 13997-14013.
- Pankhurst, R.J., Rapela, C.W., 1998. The proto-Andean margin of Gondwana: an introduction. In: Pankhurst, R.J., Rapela, C.W. (eds.). *The Proto-Andean Margin of Gondwana*. Geological Society, Special Publication, 142, 1-9.
- Pankhurst, R.J., Rapela, C.W., Fanning, C.M., Márquez, M., 2006. Gondwanide continental collision and the origin of Patagonia. *Earth Science Reviews*, 76, 235-257.
- Pearce, J.A., Haris, N.B.W., Tindle, A.G., 1984. Trace element discrimination diagrams for the tectonic interpretation of granitic rocks. *Journal of Petrology*, 25, 956-983.
- Pérez, D.J., Ramos, V.A., 1996. El basamento prejurásico. In: Ramos, V.A., Aguirre Urreta, M.B., Álvarez, P.P., Cegarra, M., Cristallini, E.O., Kay, S.M., Lo Forte, G.L., Pereira, F.X., Pérez, D.J. (eds.). *Geología de la Región del Aconcagua, Provincias de San Juan y Mendoza*. Subsecretaría de Minería de la Nación, Dirección Nacional del Servicio Geológico, Anales, 24, 27-58.
- Ramos, V.A., Kay, S.M., 1991. Triassic rifting and associated basalts in the Cuyo basin, central Argentina. In: Harmon, R.S., Rapela, C.W. (eds.). *Andean Magmatism and its Tectonic Setting*. Geological Society of America Special Paper, 265, 79-91.
- Remane, J., 2000. International stratigraphic chart and explanatory note to the international stratigraphic chart. International Union of Geological Sciences, Trondheim, 16 p.
- Sambridge, M.S., Compston, W., 1994. Mixture modelling of multicomponent data sets with application to ion-probe zircon ages. *Earth and Planetary Science Letters*, 128, 373-390.
- Spalletti, L., 1999. Cuencas triásicas del oeste argentino: origen y evolución. *Acta Geologica Hispanica* 32(1997), 29-50.
- Spalletti, L.A., 2001. Evolución de las cuencas sedimentarias. In: Artabe, A.E., Morel, E.M., Zamuner, A.E. (eds.). *El Sistema Triásico en la Argentina*. La Plata, Fundación Museo de La Plata "Francisco P. Moreno", 81-101.
- Spalletti, L., Artabe, A., Morel, E., Brea, M., 1999. Biozonación paleoflorística y cronoestratigrafía del Triásico Argentino. *Ameghiniana*, 36, 419-451.
- Spalletti, L., Morel, E., Artabe, A., Zavattieri, A., Gauza, D., 2005. Estratigrafía, facies y paleoflora de la sucesión triásica de Potrerillos, Mendoza, República Argentina. *Revista Geológica de Chile*, 32, 249-272.
- Stipanicic, P.N., 2001. Antecedentes geológicos y paleontológicos. In: Artabe, A.E., Morel, E.M., Zamuner, A.B. (eds.). *El Sistema Triásico en la Argentina. La Plata, Fundación Museo de La Plata "Francisco P. Moreno"*, 1-21.
- Stipanicic, P.N., Marsicano, C., 2002. Triásico. Léxico Estratigráfico de la Argentina (VIII). Buenos Aires, Asociación Geológica Argentina, Serie "B" Didáctica y Complementaria, 26, 370 p.
- Strazzere, L., Gregori, D.A., Dristas, J.A., 2006. Genetic evolution of Permo-Triassic volcaniclastic sequences at Uspallata, Mendoza Precordillera, Argentina. *Gondwana Research*, 8, 485-499.
- Taylor, S.R., McLennan, S.M., 1985. *The Continental Crust: its Composition and Evolution*. Oxford, Blackwell Scientific Publications, 312 pp.
- Tera, F., Wasserburg, G., 1972. U-Th-Pb systematics in three Apollo 14 basalts and the problem of initial Pb in lunar rocks. *Earth and Planetary Science Letters*, 14, 281-304.
- Vilas, J.F.A., Valencio, D.A., 1982. Implicancias geodinámicas de los resultados paleomagnéticos de formaciones asignadas al Paleozoico Tardío – Mesozoico Temprano del centro-oeste argentino. *V Congreso Latinoamericano de Geología*, Buenos Aires, Actas, 3, 743-758.
- Williams, I.S., 1998. U-Th-Pb Geochronology by Ion Microprobe. In: McKibben, M.A., Shanks III, W.C., Ridley, W.I. (eds.). *Applications of microanalytical techniques to understanding mineralizing processes*. *Reviews in Economic Geology*, 7, 1-35.
- Winchester, J.A., Floyd, P.A., 1977. Geochemical discrimination of different magma series and their differentiation products using immobile elements. *Chemical Geology*, 20, 161-179.

Manuscript received December 2007;
revision accepted March 2008;
published Online July 2008.

TABLE 1 | Geochemical analyses of the Potrerillos Formation tuffs.

SAMPLE	SiO₂	Al₂O₃	Fe₂O₃	MnO	MgO	CaO	Na₂O	K₂O	TiO₂	P₂O₅	LOI	TOTAL	CIA
PTR0	61.95	18.84	2.09	0.054	1.33	0.81	2.3	3.88	0.728	0.1	7.71	99.81	72.94
PTR1	74.02	12.38	0.94	0.012	0.12	0.2	5.82	0.61	0.216	0.03	5.36	99.71	65.12
PTR2	63.7	17.23	1.32	0.207	0.27	4.81	3.72	0.99	0.925	0.14	6.35	99.66	64.41

Sc	Be	V	Cr	Co	Ni	Cu	Zn	Ga	Ge	As	Rb	Sr
14	4	88	<20	14	<20	20	130	25	1.7	6	160	156
5	<1	8	<20	<1	<20	<10	30	10	1.3	<5	22	44
11	1	52	30	3	<20	10	90	19	1.1	<5	28	297

Y	Zr	Nb	Mo	Ag	In	Sn	Sb	Cs	Ba	La	Ce	Pr
41.9	358	14.5	<2	<0.5	<0.1	2	0.8	13.2	585	42.3	81.4	10.5
38.4	206	12.5	<2	<0.5	<0.1	2	0.4	6.9	221	33.4	69.5	9.15
27.1	274	11.1	<2	<0.5	<0.1	<1	0.2	1.8	762	35.3	65.8	8.87

Nd	Sm	Eu	Gd	Tb	Dy	Ho	Er	Tm	Yb	Lu	Hf	Ta
37.9	7.55	1.63	6.31	1.12	6.65	1.32	4.11	0.615	3.88	0.59	9.9	1.11
33.4	7.16	1.29	6.49	1.12	6.39	1.27	3.92	0.587	3.77	0.59	6.5	1.09
32.1	6.25	1.91	5.4	0.87	4.71	0.94	2.79	0.413	2.62	0.42	7.4	0.7

W	Tl	Pb	Bi	Th	U
2.2	0.94	15	0.3	14.3	4.06
4.2	0.19	19	0.4	16.6	3.79
1.6	0.17	13	<0.1	7.17	1.5

TABLE 2 | U-Pb Zircon SHRIMP Data for Sample PRT 0.

Grain spot	U (ppm)	Th (ppm)	Th/U	$^{206}\text{Pb}^*$ (ppm)	$^{204}\text{Pb}/^{206}\text{Pb}$	f_{206} %	Total		Radiogenic		Age (Ma)			
							$^{238}\text{U}/^{206}\text{Pb}$	\pm	$^{207}\text{Pb}/^{206}\text{Pb}$	\pm	$^{206}\text{Pb}/^{238}\text{U}$	\pm		
1.1	18	15	0.80	0.7	0.004460	4.78	22.946	0.650	0.0898	0.0116	0.0415	0.0014	262.1	8.5
2.1	53	34	0.64	1.7	0.000837	1.96	25.913	0.511	0.0667	0.0026	0.0378	0.0008	239.4	4.8
3.1	108	74	0.68	3.9	0.000520	0.88	23.783	0.380	0.0585	0.0017	0.0417	0.0007	263.2	4.2
4.1	184	115	0.63	6.7	-	0.34	23.424	0.335	0.0543	0.0014	0.0425	0.0006	268.6	3.8
5.1	184	119	0.65	6.5	0.000306	0.67	24.243	0.348	0.0568	0.0015	0.0410	0.0006	258.9	3.7
6.1	113	76	0.67	3.9	0.001544	0.96	24.639	0.395	0.0590	0.0033	0.0402	0.0007	254.0	4.2
7.1	252	204	0.81	8.9	0.000081	0.44	24.386	0.332	0.0549	0.0021	0.0408	0.0006	258.0	3.5
8.1	123	99	0.81	4.3	0.000599	0.81	24.461	0.375	0.0578	0.0023	0.0405	0.0006	256.2	4.0
9.1	22	16	0.71	0.8	-	3.94	23.146	0.773	0.0831	0.0091	0.0415	0.0015	262.1	9.3
10.1	27	17	0.62	1.0	0.000389	3.42	24.098	0.865	0.0786	0.0069	0.0401	0.0015	253.3	9.3
11.1	109	71	0.65	4.0	0.000446	0.79	23.324	0.369	0.0580	0.0017	0.0425	0.0007	268.5	4.2
12.1	183	172	0.94	6.0	0.000118	0.42	26.302	0.381	0.0543	0.0013	0.0379	0.0006	239.6	3.4
13.1	215	146	0.68	7.5	0.000053	0.56	24.705	0.348	0.0558	0.0014	0.0403	0.0006	254.4	3.6
14.1	202	144	0.71	7.2	0.000448	0.71	24.069	0.341	0.0572	0.0012	0.0413	0.0006	260.6	3.7
15.1	22	10	0.46	0.7	0.002992	0.91	26.674	0.717	0.0581	0.0037	0.0372	0.0010	235.1	6.3
16.1	107	104	0.98	3.7	0.001051	0.64	24.816	0.400	0.0564	0.0025	0.0400	0.0007	253.1	4.1
17.1	77	39	0.51	2.9	0.001480	1.18	22.559	0.388	0.0613	0.0029	0.0438	0.0008	276.4	4.8
18.1	96	35	0.36	3.6	0.000963	0.47	23.146	0.374	0.0554	0.0016	0.0430	0.0007	271.4	4.4
19.1	13	8	0.59	0.5	0.010689	7.78	21.738	0.765	0.1140	0.0140	0.0424	0.0018	267.8	10.9
20.1	47	23	0.49	1.7	0.001586	1.30	23.254	0.460	0.0621	0.0046	0.0424	0.0009	268.0	5.5
21.1	211	156	0.74	8.2	0.000482	0.22	22.214	0.308	0.0537	0.0011	0.0449	0.0006	283.3	3.9
22.1	38	35	0.91	1.7	0.003792	4.94	18.936	0.428	0.0924	0.0070	0.0502	0.0013	315.8	7.8
23.1	73	37	0.51	2.6	0.000144	0.85	23.879	0.416	0.0583	0.0019	0.0415	0.0007	262.3	4.6
24.1	25	13	0.51	0.9	0.003935	1.23	23.582	0.553	0.0614	0.0030	0.0419	0.0010	264.5	6.2
25.1	65	28	0.43	2.4	0.001346	0.98	23.258	0.391	0.0595	0.0022	0.0426	0.0007	268.8	4.5
26.1	67	40	0.59	2.2	0.000257	1.08	26.071	0.436	0.0596	0.0023	0.0379	0.0006	240.1	4.0
27.1	310	143	0.46	11.3	0.000276	<0.01	23.483	0.277	0.0511	0.0008	0.0426	0.0005	269.0	3.1
28.1	225	295	1.31	8.1	-	0.34	23.835	0.448	0.0542	0.0009	0.0418	0.0008	264.1	4.9

Notes:

1. Uncertainties given at the 1- σ level.
2. Error in FC1 reference zircon calibration was 0.58% and 0.27% (at 95% c.l.) for the analytical sessions (not included in above errors but required when comparing data from different mounts).
3. – denotes that no ^{204}Pb was detected
4. f_{206} % denotes the percentage of ^{206}Pb that is common Pb.
5. Correction for common Pb made using the measured $^{238}\text{U}/^{206}\text{Pb}$ and $^{207}\text{Pb}/^{206}\text{Pb}$ ratios following Tera and Wasserburg (1972), as outlined in Williams (1998; the so called ^{207}Pb correction method).

TABLE 3 | U-Pb Zircon SHRIMP Data for Sample PTR 1.

Grain. spot	U (ppm)	Th (ppm)	Th/U	$^{206}\text{Pb}^*$ (ppm)	$^{204}\text{Pb}/^{206}\text{Pb}$	f_{206} %	Total			Radiogenic			Age (Ma)	
							$^{238}\text{U}/^{206}\text{Pb}$	\pm	$^{207}\text{Pb}/^{206}\text{Pb}$	\pm	$^{206}\text{Pb}/^{238}\text{U}$	\pm	$^{206}\text{Pb}/^{238}\text{U}$	\pm
1.1	14	11	0.73	0.6	0.009493	8.24	21.132	0.614	0.1179	0.0090	0.0434	0.0015	274.0	9.0
2.1	701	357	0.51	25.7	0.000078	<0.01	23.411	0.254	0.0515	0.0005	0.0427	0.0005	269.7	2.9
3.1	44	39	0.89	1.4	0.001902	1.54	26.612	0.520	0.0632	0.0029	0.0370	0.0007	234.2	4.6
4.1	117	60	0.51	4.3	0.000276	0.31	23.457	0.335	0.0541	0.0013	0.0425	0.0006	268.3	3.8
5.1	76	114	1.50	2.5	0.000548	1.01	26.479	0.436	0.0590	0.0026	0.0374	0.0006	236.6	3.9
6.1	272	143	0.53	9.8	0.000303	0.42	23.871	0.287	0.0548	0.0009	0.0417	0.0005	263.5	3.1
7.1	81	112	1.39	2.7	0.000226	0.67	25.976	0.405	0.0564	0.0023	0.0382	0.0006	241.9	3.8
8.1	131	233	1.78	4.2	-	0.64	26.511	0.400	0.0560	0.0020	0.0375	0.0006	237.2	3.6
9.1	183	105	0.57	5.9	0.000125	0.41	26.393	0.350	0.0543	0.0010	0.0377	0.0005	238.8	3.1
10.1	126	219	1.73	4.2	0.000156	0.64	25.873	0.363	0.0562	0.0013	0.0384	0.0005	242.9	3.4
11.1	118	196	1.66	3.9	0.000425	0.49	25.778	0.363	0.0550	0.0013	0.0386	0.0006	244.2	3.4
12.1	54	62	1.15	1.8	-	1.47	26.378	0.478	0.0626	0.0022	0.0374	0.0007	236.4	4.3
13.1	26	11	0.44	1.0	0.000926	2.80	23.514	0.551	0.0739	0.0059	0.0413	0.0010	261.1	6.4
14.1	161	189	1.18	5.2	0.000468	0.53	26.421	0.357	0.0552	0.0019	0.0376	0.0005	238.2	3.2
15.1	79	108	1.36	2.6	0.000578	1.21	26.097	0.516	0.0607	0.0039	0.0379	0.0008	239.5	4.8
16.1	150	94	0.62	5.1	0.000040	0.44	25.252	0.340	0.0547	0.0022	0.0394	0.0005	249.3	3.4
17.1	175	121	0.69	5.9	0.000650	0.16	25.345	0.331	0.0524	0.0012	0.0394	0.0005	249.1	3.2
18.1	63	80	1.26	2.2	0.001957	1.57	24.783	0.448	0.0638	0.0023	0.0397	0.0007	251.1	4.6
19.1	363	422	1.16	11.9	0.000179	0.27	26.119	0.304	0.0532	0.0008	0.0382	0.0004	241.6	2.8
20.1	68	46	0.68	2.5	0.001119	0.81	22.967	0.379	0.0582	0.0021	0.0432	0.0007	272.6	4.5

Notes:

1. Uncertainties given at the $1-\sigma$ level.
2. Error in FC1 reference zircon calibration was 0.27% (at 95% c.l.) for the analytical session
(not included in above errors but required when comparing data from different mounts).
3. – denotes that no ^{204}Pb was detected
4. f_{206} % denotes the percentage of ^{206}Pb that is common Pb.
5. Correction for common Pb made using the measured $^{238}\text{U}/^{206}\text{Pb}$ and $^{207}\text{Pb}/^{206}\text{Pb}$ ratios following Tera and Wasserburg (1972),
as outlined in Williams (1998; the so called ^{207}Pb correction method).

TABLE 4 | U–Pb Zircon SHRIMP Data for sample PTR 2.

Grain. spot	U (ppm)	Th (ppm)	Th/U	$^{206}\text{Pb}^*$ (ppm)	$^{204}\text{Pb}/$ ^{206}Pb	f_{206} %	Total		Radiogenic		Age (Ma)			
							$^{238}\text{U}/$ ^{206}Pb	\pm	$^{207}\text{Pb}/$ ^{206}Pb	\pm	$^{206}\text{Pb}/$ ^{238}U	\pm		
1.1	72	62	0.86	2.2	0.000882	1.05	27.900	0.500	0.0590	0.0038	0.0355	0.0007	224.7	4.1
2.1	68	82	1.20	2.2	0.001803	0.84	26.613	0.481	0.0576	0.0022	0.0373	0.0007	235.8	4.3
3.1	66	60	0.92	2.1	0.002163	1.05	27.411	0.502	0.0591	0.0022	0.0361	0.0007	228.6	4.2
4.1	85	67	0.79	2.7	0.001847	0.84	27.030	0.463	0.0575	0.0019	0.0367	0.0006	232.3	4.0
5.1	72	90	1.25	2.3	0.001309	0.95	27.469	0.488	0.0583	0.0021	0.0361	0.0007	228.4	4.1
6.1	56	52	0.93	1.7	-	2.16	27.784	0.791	0.0679	0.0030	0.0352	0.0010	223.1	6.4
7.1	62	61	0.98	1.9	0.001312	1.43	27.748	0.515	0.0621	0.0046	0.0355	0.0007	225.0	4.3
8.1	127	137	1.08	4.0	0.000004	0.53	27.492	0.424	0.0550	0.0021	0.0362	0.0006	229.1	3.6
9.1	133	235	1.77	4.2	0.000014	0.74	27.257	0.417	0.0567	0.0025	0.0364	0.0006	230.6	3.6
10.1	65	72	1.10	2.1	-	1.18	27.200	0.504	0.0602	0.0035	0.0363	0.0007	230.0	4.3
11.1	87	124	1.43	2.7	-	0.78	27.377	0.612	0.0570	0.0021	0.0362	0.0008	229.5	5.1
12.1	66	55	0.84	2.1	-	1.00	26.374	0.483	0.0589	0.0040	0.0375	0.0007	237.6	4.5
13.1	178	211	1.19	5.7	0.000282	0.59	26.955	0.392	0.0556	0.0019	0.0369	0.0005	233.5	3.4
14.1	78	86	1.10	2.5	0.000937	1.19	26.298	0.459	0.0605	0.0035	0.0376	0.0007	237.8	4.2
15.1	63	49	0.78	2.0	0.000857	1.48	27.034	0.502	0.0627	0.0052	0.0364	0.0007	230.7	4.5
16.1	67	66	0.99	2.0	-	1.00	28.047	0.520	0.0586	0.0029	0.0353	0.0007	223.6	4.2
17.1	66	62	0.93	2.1	0.002012	1.20	27.467	0.503	0.0603	0.0045	0.0360	0.0007	227.8	4.3
18.1	38	33	0.86	1.2	0.001024	2.64	27.407	0.604	0.0718	0.0037	0.0355	0.0008	225.0	5.1
19.1	65	65	0.99	2.1	0.001131	0.76	26.233	0.632	0.0571	0.0023	0.0378	0.0009	239.4	5.7
20.1	68	60	0.89	2.2	0.001367	1.93	26.722	0.487	0.0663	0.0031	0.0367	0.0007	232.3	4.3

Notes:

1. Uncertainties given at the 1σ level.
- 2a. Error in FC1 reference zircon calibration was 0.58% (at 95% c.l.) for the analytical session
(not included in above errors but required when comparing data from different mounts).
3. – denotes that no ^{204}Pb was detected
4. f_{206} % denotes the percentage of ^{206}Pb that is common Pb.
5. Correction for common Pb made using the measured $^{238}\text{U}/^{206}\text{Pb}$ and $^{207}\text{Pb}/^{206}\text{Pb}$ ratios following Tera and Wasserburg (1972), as outlined in Williams (1998; the so called ^{207}Pb correction method).